Translational ^{18}F-FDG PET/CT Imaging to Monitor Lesion Activity in Intestinal Inflammation

Dominik Bettenworth*[1], Stefan Reuter*[2], Sven Hermann[3,4], Matthias Weckesser[4], Linda Kerstiens[5], Athanasios Stratis[6], Tobias Max Nowacki[1], Matthias Ross[1], Frank Lenze[1], Bayram Edemir[2], Christian Maaser[7], Thomas Pap[6], Steffen Koschmieder[5], Jan Heidemann[1], Michael Schäfers*[4], and Andreas Lügering*[1]

[1]Department of Medicine B, University of Münster, Münster, Germany; [2]Department of Medicine D, University of Münster, Münster, Germany; [3]European Institute for Molecular Imaging, University of Münster, Münster, Germany; [4]Department of Nuclear Medicine, University of Münster, Münster, Germany; [5]Department of Medicine A, University of Münster, Münster, Germany; [6]Institute for Experimental Musculoskeletal Medicine University of Münster, Münster, Germany; and [7]University Teaching Hospital Lüneburg, Lüneburg, Germany

In patients with inflammatory bowel disease (IBD) and in murine IBD models, mucosal disease activity is routinely assessed by endoscopy and histologic evaluation. This information is valuable for monitoring treatment response, with mucosal healing being a major treatment goal. The aim of this study was to evaluate the translational potential of noninvasive ^{18}F-FDG PET/CT for the assessment of mucosal damage in murine dextran sodium sulfate (DSS) colitis and human IBD. **Methods:** After induction of DSS colitis, ^{18}F-FDG uptake was serially assessed from colonic volumes of interest defined on PET/CT scans and intraindividually correlated to histologic findings and to infiltrating cell types. In addition, ^{18}F-FDG PET/CT scans of 25 Crohn disease patients were analyzed, and colonic ^{18}F-FDG uptake was correlated to endoscopically assessed damage. **Results:** At days 4 and 7 after DSS induction, colonic ^{18}F-FDG uptake was significantly increased, with a distinct peak in the medial colon. ^{18}F-FDG uptake strongly correlated with histologic epithelial damage. Additionally, ^{18}F-FDG uptake increased in the bone marrow in the course of the disease, correlating with an increase in intestinal ^{18}F-FDG uptake. Histology and fluorescence-activated cell sorting analysis of the bone marrow of DSS mice revealed an increased number of immature neutrophils, whereas mucosal polymerase chain reaction suggested a correlation of ^{18}F-FDG uptake to T cell infiltration. In accordance with the results of ^{18}F-FDG PET/CT in DSS colitis, an increased ^{18}F-FDG uptake was found in 87% of deep mucosal ulcerations in IBD patients, whereas mild endoscopic lesions were detected only by ^{18}F-FDG PET/CT in about 50% of patients assessed. **Conclusion:** ^{18}F-FDG PET/CT is a noninvasive method for evaluation of both experimental colitis and Crohn disease patients and thereby offers promising translational potential.

Key Words: inflammatory bowel disease; ^{18}F-FDG PET/CT; murine colitis

J Nucl Med 2013; 54:748–755
DOI: 10.2967/jnumed.112.112623

Types of inflammatory bowel disease (IBD) such as Crohn disease and ulcerative colitis are chronic-remittent, inflammatory conditions, featuring characteristic mucosal lesions within the bowel leading to diarrhea, stricture formation, abdominal pain, and weight loss (*1*). Frequently, extraintestinal manifestations such as arthritis occur (*2,3*). The evaluation of disease activity is critical for both initiation and monitoring of drug treatment. Although chronic and usually severe local intestinal infiltration by activated immune cells is typically evident, systemic inflammatory parameters such as C-reactive protein are of limited informative value and do not correlate well with the extent of the disease (*1,4*). The value of other biomarkers such as calprotectin still needs to be established. Thus, endoscopic evaluation with subsequent biopsies followed by histologic investigation still remains a critical procedure for the diagnosis and follow-up of IBD (*1*). However, variation of localization and the dynamics of inflammation in the course of the disease and complications such as progression to stricture and abscess formation might limit the performance of this procedure (*2*). Moreover, serial colonoscopy procedures that are required to monitor disease activity are invasive and uncomfortable for patients. Because treatment of IBD has been focused toward a tight control of disease activity to avoid disease progression and functional impairment of the bowel, the appropriate method for disease monitoring still needs to be determined. In this context, mucosal healing as assessed by colonoscopy has been established as a marker widely used in clinical trials (*5,6*). However, because Crohn disease transmurally involves the complete intestinal tract, more enhanced imaging methods are deemed necessary.

Received Aug. 12, 2012; revision accepted Nov. 26, 2012.
For correspondence or reprints contact: Dominik Bettenworth, Department of Medicine B, University of Münster, D-48149 Münster, Germany.
E-mail: dominik.bettenworth@ukmuenster.de
*Contributed equally to this work.
Published online Mar. 20, 2013.

Animal models of intestinal inflammation have contributed substantially to the current understanding of IBD and are widely used for preclinical drug testing (*7,8*). Because endoscopic examinations are complicated in the assessment of small-animal IBD, other clinical surrogate markers such as weight loss have to be used to avoid necropsy. Obviously, unspecific parameters such as weight loss do not reflect intestinal inflammation alone. Therefore, a noninvasive tool for repeated detection and quantification of IBD activity that can be applied serially in small animals is desirable. To this end, ^{18}F-FDG PET/CT has been reported for the evaluation of dextran sodium sulfate (DSS) colitis recently (*9*).

Clinical ^{18}F-FDG PET/CT is a noninvasive imaging modality widely used for detection, staging, and follow-up of tumors, infections, and sterile inflammation (*10*). In preliminary studies, ^{18}F-FDG PET has shown promising results for the assessment of inflammation in adult and pediatric patients with IBD (*11,12*). However, because of the limited knowledge regarding its implication for treatment decisions, the method is not routinely used for determining disease activity.

Murine DSS colitis is a valid, well-characterized standard experimental model of IBD (*7,8,13–15*). DSS primarily causes intestinal epithelial cell damage, resulting in a robust inflammatory response, which includes a massive infiltration of activated leukocytes into the colonic wall lasting several days to weeks. Activated leukocytes show a distinct accumulation of ^{18}F-FDG, which can be measured by PET (*16,17*). In this study, we evaluated ^{18}F-FDG PET/CT as a method for the assessment of DSS colitis and correlated the signals obtained to ^{18}F-FDG PET/CT findings in patients with endoscopic evidence of colonic Crohn disease inflammatory activity.

MATERIALS AND METHODS

Animals and DSS Colitis

C57BL/6 wild-type (WT) (age, 6–8 wk, at the beginning of the experiments) female mice were purchased from Charles River Laboratories. In initial experiments, no major sex-specific differences could be detected in the course of colitis. Therefore, experiments described here were conducted using female mice for practical reasons only. All animals were kept under pathogen-free conditions at 24°C with a controlled 12-h day–night cycle and had free access to a standard diet and drinking water. All animal studies were approved by a governmental committee on animal welfare and were performed in accordance with national animal protection guidelines.

DSS colitis was induced as described previously (*18*). In brief, mice were given 3% DSS (ICN Biomedicals Inc.) in drinking water for 6 d, and disease activity was monitored daily by body weight measurement. Afterward, the mice received regular drinking water again to monitor the improvement of inflammation. At the end of the experiment, mice were sacrificed and the colons removed. Colons were opened, embedded in optimal-cutting-temperature compound (Tissue Tek; Sakura Fine Tek Europe), and kept frozen at −80°C until further use. Frozen sections (5 μm) were stained with hematoxylin and eosin and analyzed in a masked manner by 2 investigators.

^{18}F-FDG PET and ^{18}F-FDG PET/CT of C57Bl6 WT Mice

PET experiments were performed using a submillimeter high-resolution (0.7 mm in full width at half maximum) small-animal scanner (32 module quadHIDAC; Oxford Positron Systems Ltd.) with a uniform spatial resolution (<1 mm) over a large cylindric field (165-mm diameter, 280-mm axial length) (*19*).

Mice were anesthetized with oxygen–isoflurane inhalation (2% isoflurane, 0.4 l/min oxygen), and body temperature was maintained at physiologic values by a heating pad. One hour after the intravenous injection of 10 MBq of ^{18}F-FDG in 100 μL of 0.9% saline, list-mode data were acquired for 15 min. Subsequently, the scanning bed was transferred to the CT scanner (Inveon; Siemens Medical Solutions), and after intravenous injection of a contrast agent (5 μL/g of body weight; Ultravist 300 [Bayer HeathCare]) a CT image with a spatial resolution of approximately 80 μm was obtained for each mouse. A subgroup of mice was sacrificed immediately after the in vivo PET. The colon was removed, cut lengthwise, unrolled, and rinsed, and an ex vivo PET image was acquired for 10 min. Reconstructed in vivo image datasets were coregistered using extrinsic markers attached to the multimodal scanning bed and the image analysis software (Inveon Research Workplace 3.0; Siemens Medical Solutions).

Analysis of PET Images and Quantitative Evaluation

In Vivo PET. Three-dimensional volumes of interest (VOIs) in the parenchyma were defined in CT datasets for the proximal, medial, and distal colon. Subsequently, the VOIs were transferred to the coregistered PET data and analyzed quantitatively. Regional uptake was calculated as percentage of injected dose by dividing counts per second per milliliter in the VOI by total counts per second in the mouse multiplied by 100 (%ID/mL).

Ex Vivo PET. On the basis of the standardized removal of the colon, six 3-dimensional VOIs were defined starting from the proximal end (length, VOIs 1–5: 1 cm each; VOI 6: remaining rectum). VOI uptake was calculated as counts per second per milliliter.

Histologic Evaluation

Histologic analysis of the proximal, medial, and distal colon focused on epithelial denudation, ulceration, edema, and leukocyte infiltrates. For DSS colitis, 3 colonic sections of each animal were scored in a masked fashion by 2 experienced examiners using a colitis score as previously described by Dieleman et al. (*14*). In brief, for each category of the score (inflammation, extent, crypt damage), points were multiplied by a factor of involvement of the visible epithelium. The sum of the 3 category scores added up to the total score of a section (0–40 points). The average of the 3 colon sections was representative for each animal. The analysis reached high interobserver agreement.

Analysis of Epithelial Damage and Cellular Infiltrate of Colonic Mucosal Sections

In another set of experiments, in vivo and ex vivo PET of the colon were performed as described above. Subsequently, colons were divided longitudinally and then cut through every centimeter according to VOIs previously defined by PET. Every centimeter piece was again divided and transferred to hematoxylin and eosin staining (to evaluate epithelial damage) and to polymerase chain reaction (PCR) analysis to evaluate for perforin expression (primer sequences sense/antisense: 5′ GCA GCT GAG AAG ACC TAT

CAG-3′, 5′-AGG AGA TGA GCC TGT GGT AAG C-3′), CD66 (5′-CAA TGT CAC GAG GAA TGA CAC AGG-3′, 5′-CTG CAT GGC AGG AGA GGT TG-3′), Ficolin B (5′- GGA GAT AGA GGA GAG AGT GGC-3′, 5′-CCT GGG TGA GCA ACT CCT TGC-3′), and MAdCAM-1 (5′-GGC GAC CTG GCA ACC time–activity curve CAC-3′, 5′- CCCAGCACCAAGCTGCCAATC-3′). Expression profiles of selected marker genes were validated by real-time PCR, which was performed using SYBR Green PCR Master Mix or TaqMan Universal PCR Master Mix on an ABI PRISM 7700 Sequence Detection System. Specific primer pairs were used. All instruments and reagents were purchased from Applied Biosystems. Relative gene expression values were evaluated with the $2^{-\Delta\Delta Ct}$ method using glyceraldehyde-3-phosphate dehydrogenase as a housekeeping gene.

Toluidine Blue Staining of Joints

Tissue samples from joints of healthy and DSS-treated C57Bl6 WT mice were fixed in 4% paraformaldehyde, decalcified in 10% ethylenediaminetetraacetic acid/phosphate-buffered saline, and embedded into paraffin, and 5-μm sections were stained with Toluidine blue as described previously (*20*).

Histology

Mice were sacrificed by CO_2 inhalation, and organs were removed and fixed in neutrally buffered 10% formalin at room temperature for 16 h before they were embedded in paraffin and sectioned. All tissues were stained with hematoxylin and eosin or naphthylacetate for light microscopy as indicated. Light microscopy was performed with an Axioplan microscope (Zeiss) using a 25x Plan-Neofluar 0.80, 63x Plan-Apochromat 1.4 oil, or 100x Plan-Neofluar 1.30 oil lens. Images were captured using Adobe Photoshop (version 5.5; Adobe Systems).

Analysis of Flow Cytometry

Bone marrow and spleen cells were isolated as described previously (*21*). Lysis of enucleated red blood cells was achieved by applying ammonium-chloride-potassium buffer. After being washed, cells were analyzed using a FACScalibur cytometer (BD Biosciences) after incubation with the following antibodies: murine CD3, B220, Gr-1, Ter119, and CD11b antibodies (Invitrogen).

Analysis of ^{18}F-FDG PET/CT Images of IBD Patients

Twenty-five patients with histologically diagnosed Crohn colitis for at least 6 mo were included (Table 1 shows demographic and clinical characteristics). A hybrid PET/CT scanner (Biograph Sensation 16; Siemens) was used for data acquisition. After a fasting period of at least 8 h, a body mass–adapted ^{18}F-FDG activity of 4 MBq/kg of body weight was injected intravenously. Images were acquired 1 h later. Injected ^{18}F-FDG activities and x-ray radiation doses of the CT scanner were reduced to the necessary minimum. The maximum-pixel-value standardized uptake value (SUV_{max}), normalized for body weight, according to previously published data, was used. Lesions with an SUV_{max} of 4.0 and higher were defined as positive findings (*22*). All studies were performed under the approval of the Institutional Review Board for Human Investigation at the University Hospital of Münster after written informed consent was obtained.

Endoscopic Scoring of Inflammation

The colonoscopic examinations were evaluated for the extent of inflammation in 5 ileocolonic segments (ileocecum, ascending colon, colon transversum, descending colon, and rectosigmoid). Extent of inflammation was scored from 0 to 3 defined as 0 (no inflammatory changes), 1 (erythematous mucosa), superficial ulceration (2), and deep ulceration (3) in accordance with the Crohn Disease Endoscopic Index of Severity (*23*).

TABLE 1
Demographic and Clinical Characteristics of Crohn Disease Patients

Characteristic	Data
Sex	
Female	11 (44)
Male	14 (56)
Age (y)	40.2 ± 3.1
Duration of disease (y)	13.3 ± 2.2
Crohn disease activity index	222.4 ± 24.1
C-reactive protein level (mg/dL)	2.4 ± 0.6
Immunosuppressive treatment	13 (52)

Data are *n* or mean ± SD, with percentages in parentheses.

Statistical Analysis

Data were compared by a 2-way ANOVA with a Bonferroni multiple-comparisons test, Student *t* test, and assessment of correlation according to Pearson, where appropriate. Data are presented as mean values ± SE (n = number of patients, mice, samples, or experiments). Significance was inferred at the P less than 0.05 level.

RESULTS

^{18}F-FDG PET/CT in Murine DSS Colitis

After the administration of DSS, all mice developed progressive diarrhea. As expected, weight loss started on day 4 and peaked on day 8 (Fig. 1A). After DSS treatment was stopped, mice regained weight from day 8 on. The colon length was significantly shorter (8.2 ± 0.3 cm [control] vs. 6.6 ± 0.2 cm [day 7] vs. 5.6 ± 0.3 cm [day 10], $n = 6$, $P < 0.05$) in treated mice than in healthy controls. Compared with control mice, we detected a clearly elevated ^{18}F-FDG uptake in the colon of DSS-treated mice at day 7 (Fig. 1B), with the most intensive area of ^{18}F-FDG uptake in the medial and distal colon, compared with the proximal colon (Fig. 1B). In the next step, we applied ex vivo PET to further prove ^{18}F-FDG PET data obtained in vivo, revealing an excellent correlation between ex vivo and in vivo results. By using 3-dimensional CT reconstructions coregistered to PET, corresponding anatomic structures could be identified in vivo, allowing a more precise determination of regional differences found in the colon. Therefore, ^{18}F-FDG PET/CT was used for further analysis.

Quantification of Colitis Activity by ^{18}F-FDG PET/CT

In the next set of experiments, we correlated colitis activity as determined by histologic damage to ^{18}F-FDG PET/CT. To this aim, histologic damage as determined by the Dieleman score was separately analyzed on day 7 after DSS exposure in 3 different parts of the colon (proximal, medial, and distal colon). Colitis histologically presented

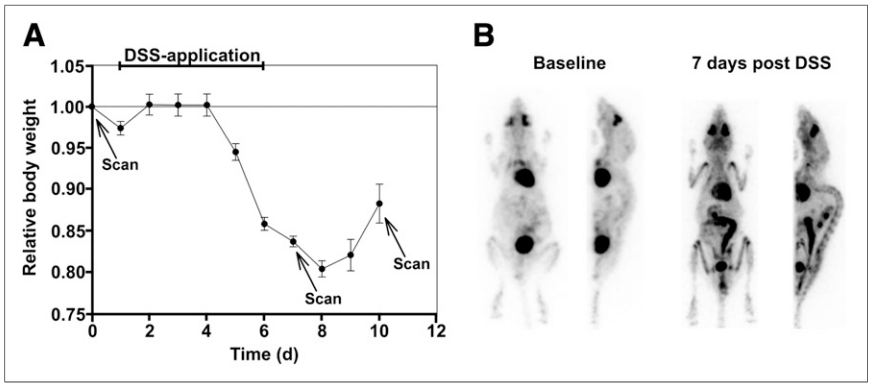

FIGURE 1. Course of DSS colitis as displayed by loss of body weight and ^{18}F-FDG PET/CT. (A) C57BL/6 WT mice received 3% DSS in drinking water for 6 d and inflammation was monitored by daily measurement of individual weights. PET/CT scans were obtained before and at 7 and 10 d after start of DSS application. Data are mean ± SE; $n = 6$ for each group. (B) Before start of DSS application, PET showed only low level of physiologic ^{18}F-FDG uptake in colon of healthy controls. In contrast, on day 7, we detected clearly elevated ^{18}F-FDG uptake. PET images are shown as maximum-intensity projections. *$P < 0.05$.

with mucosal ulceration, crypt dropout, and distinct mononuclear cell infiltration extending throughout the mucosal layer and in part the submucosal layer. Subanalysis of regional histologic activity of the proximal, medial, and distal colon revealed significant differences, with a pronounced disease in the medial colon (histologic damage, 26.8 ± 1.8 arbitrary units [AU]), a partially decreased activity in the distal colon (19.2 ± 2.9 AU; $P = 0.059$), and a significantly less active disease in the proximal colon (3 ± 0.9 AU, $P = 0.008$; Fig. 2A). Furthermore, the histologic damage in the proximal colon, as compared with the distal colon, was significantly decreased ($P < 0.01$).

In vivo ^{18}F-FDG PET/CT was performed on the same day in all mice. ^{18}F-FDG uptake analysis exhibited a most pronounced uptake in the medial colon (247.7 ± 39.9 %ID/mL change, baseline vs. day 7 after DSS start), somewhat less uptake in the distal colon (217.4 ± 41.1 %ID/mL change), and limited uptake in the proximal colon (176.2 ± 29.2 %ID/mL change, Fig. 2B). As compared with the proximal colon, the increase of ^{18}F-FDG uptake in the medial colon was elevated ($P = 0.05$).

In the following experiment, we compared individual results from the whole colon as obtained by histology and ^{18}F-FDG PET/CT and found a significant correlation between these parameters ($R^2 = 0.69$, $P < 0.05$, Fig. 2C).

Finally, we addressed whether changes in colitis activity over time can be assessed by ^{18}F-FDG PET/CT. To this aim, we compared ^{18}F-FDG PET/CT activity at day 7 (end of DSS application and reflecting the maximum of inflammation) with the activity at day 10 (recovery phase from colitis). Analyzing the medial colon as the most affected region, we detected a clearly elevated ^{18}F-FDG uptake (260.4 ± 13.1 %ID/mL change vs. baseline, $P < 0.001$) on day 7. On day 10, the ^{18}F-FDG uptake in the medial colon was still enhanced,

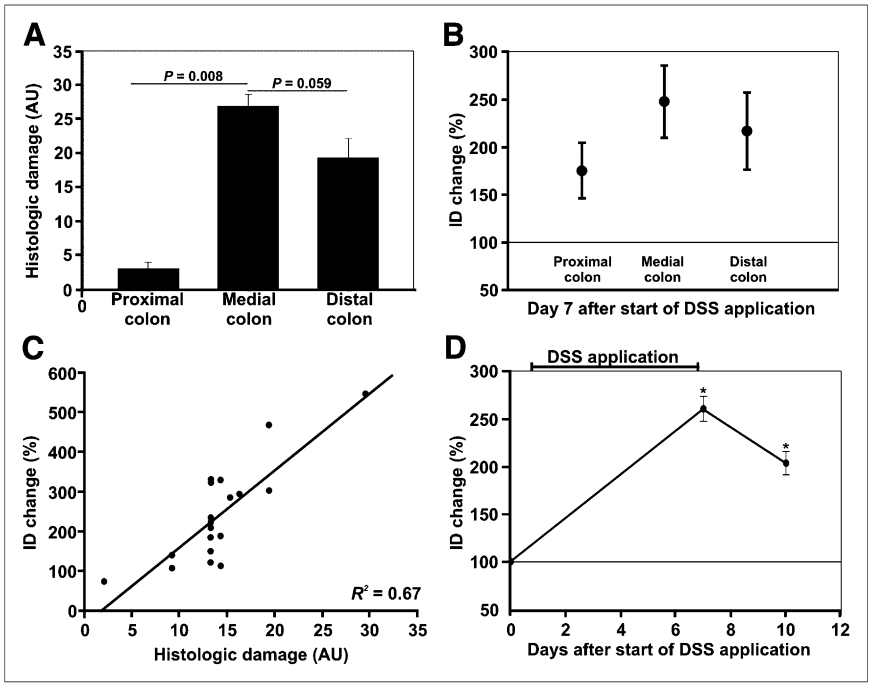

FIGURE 2. Local assessment of disease activity and correlation with histologic damage. (A) Histologic inflammatory activity in murine colonic segments 7 d after start of DSS application. (B) Relative change in regional uptake of ^{18}F-FDG along murine colon 7 d after start of DSS application, as compared with baseline scans. (C) Correlation of change in ^{18}F-FDG uptake in colon with regional histologic damage according to Dieleman score (*14*). (D) Changes of ^{18}F-FDG uptake in medial murine colon in course of DSS colitis. Data are mean ± SE; $n = 6$ for each group. *$P < 0.001$. ID = injected dose.

compared with baseline (203.4 ± 12.1 %ID/mL change, $P < 0.001$), but markedly lower than uptake on day 7 ($P < 0.01$, Fig. 2D). In the distal colon, the ^{18}F-FDG uptake on day 7 and day 10, as compared with baseline, was increased by trend ($P > 0.05$). Furthermore, evaluation of ^{18}F-FDG uptake in the proximal colon revealed neither significant increase nor increase by trend over the course of colitis.

Activation of Immature Granulocytes in Bone Marrow

Interestingly, we observed symmetric-intense ^{18}F-FDG uptake within multiple large joints (pronounced in shoulder and knee) of colitic mice. A 3.5-fold-higher ^{18}F-FDG uptake was assessed in the big joints (e.g., knee) of colitic mice than in control mice (Fig. 3A). There was a strong correlation between the relative increase of colonic and knee–shoulder articular ^{18}F-FDG uptake ($r = 0.82$, $P = 0.01$).

However, ^{18}F-FDG as a surrogate marker for cellular glucose metabolism is a rather unspecific radiotracer and therefore does not allow discrimination of colitis-induced arthritis and bone marrow activation. We therefore analyzed multiple joints by histology for signs of arthritis (Fig. 3B). None of the joints analyzed showed any signs of immune cell infiltration or cartilage damage at any time point assessed.

We next hypothesized that the elevated ^{18}F-FDG uptake may be related to systemic bone marrow activation. Bone marrow histology (Supplemental Fig. 1; supplemental materials are available online only at http://jnm.snmjournals.org) revealed massive hyperproliferation consonant with proinflammatory activation. This observation was further underscored by flow cytometric analysis of bone marrow and spleens. Using this technique, we confirmed a significant expansion of neutrophils of colitic mice, with an increase of the percentage of Gr1$^+$/CD11b$^+$ cells found within the bone marrow and in spleen cells ($P = 0.04$ and 0.009, respectively; Fig. 4). Particularly, the percentage of immature granulocytic cells (Gr1^{low}/CD11b$^+$) was significantly increased in the bone marrow of colitic mice ($P = 0.02$) but not in the spleen. Colitic mice also showed a small but significant decrease of B220$^+$ B and CD3$^+$ T cells in the bone marrow ($P < 0.001$). There was no significant difference in Ter119$^+$ erythrocytic or CD41$^+$ megakaryocytic cell counts in the bone marrow or spleen. Furthermore, the spleen weights did not differ between the 2 groups. No obvious difference in liver histology or gross follicular architecture of the spleen could be detected (data not shown).

Correlation of Mucosal Lesions to ^{18}F-FDG PET Activity

Finally, we sought to determine which inflammation-associated parameter correlated best to ^{18}F-FDG uptake in murine colitis and human colonic Crohn disease. In the murine model, we first used in vivo ^{18}F-FDG PET/CT activity and correlated the histologic damage according to each colonic segment (proximal, medial, and distal). The extent of mucosal defects was categorized into minor inflammation (without epithelial cell damage), superficial ulceration (limited to the submucosa), and extensive ulceration (ulcers

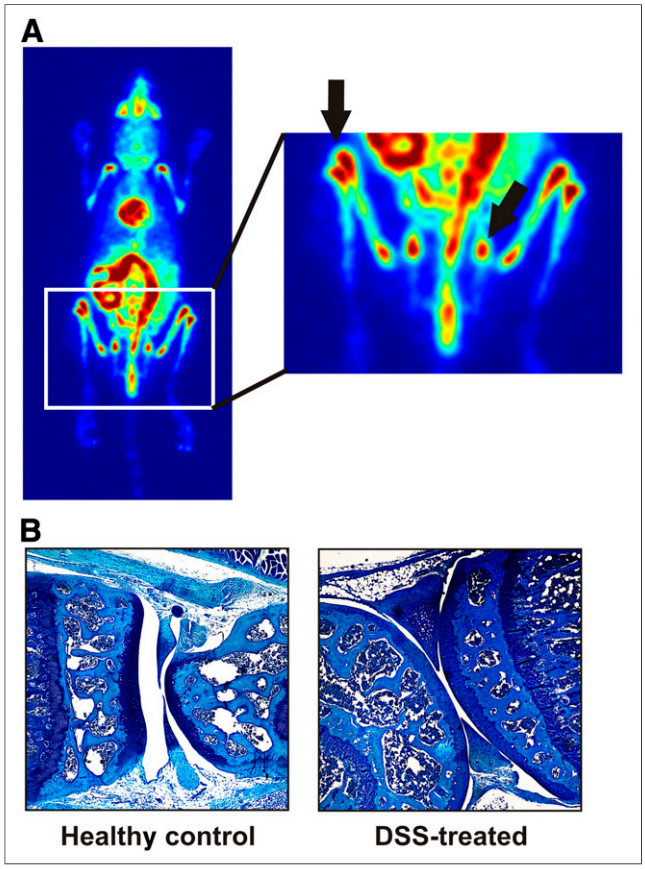

FIGURE 3. Extraintestinal findings during course of DSS colitis. (A) Whole-body ^{18}F-FDG PET (maximum-intensity projections) revealed increased uptake of ^{18}F-FDG in bone marrow 10 d after start of DSS application. (B) Toluidine blue staining of knee joints 10 d after start of DSS application. Depicted are representative images, showing no signs of immune cell infiltration or cartilage damage.

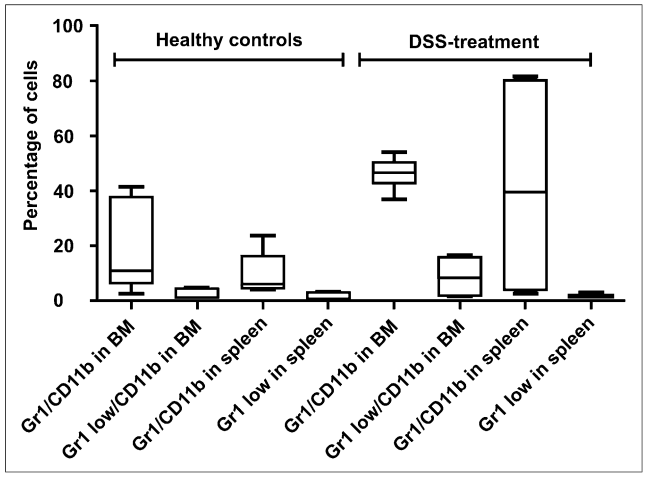

FIGURE 4. Characterizing inflammatory changes of murine bone marrow (BM). Fluorescence-activated cell sorting analysis of bone marrow and spleen of healthy WT mice and 10 d after start of DSS application. Data are mean ± SE; $n = 8$ for each group.

reaching the muscularis propria) at day 10 after colitis was induced and as confirmed by histology. By using this approach, the extent of the mucosal damage correlated significantly with the observed increase in ^{18}F-FDG uptake. For example, as compared with baseline, the increase of ^{18}F-FDG uptake for minor inflammation was 24.1% ± 13.6% ($P < 0.05$). In addition, the increase for superficial ulcerations was 86.3% ± 33.2% ($P < 0.05$) and at maximum for deep ulcerations, with an increase of 131% ± 23.7% ($P < 0.001$). To confirm this finding, we performed a more detailed analysis by measuring ex vivo ^{18}F-FDG uptake and histologic damage for every 10-mm section of the colon. By using this approach, we observed a strong correlation between epithelial damage and the ^{18}F-FDG uptake measured ex vivo, analyzing the 1-cm murine colon pieces (Fig. 5A). The mean ^{18}F-FDG uptake was 423.9 ± 43.2 counts/s/mL (MBq/g BW) in segments with intact epithelium. However, the ^{18}F-FDG uptake significantly increased to 1,562.3 ± 301.8 counts/s/mL (MBq/g BW) in areas with superficially eroded or deeply ulcerated apical epithelial layers ($P < 0.001$, Fig. 5B).

To further address the question whether the increased ^{18}F-FDG uptake in the colon was associated with the amount of T cells, as hypothesized above, real-time PCR analysis for relative expression of perforin in colonic pieces was performed. Interestingly, relative perforin expression indicating mucosal T cell infiltration correlated well with the mean activity per region of interest ($r = 0.56$, $P = 0.02$; Fig. 5C). In addition, mucosal TNF-α, IL-4, IL-10, and IL-17 expression was analyzed using real-time PCR and showed a significant correlation to intestinal ^{18}F-FDG uptake.

For human disease, we retrospectively analyzed ^{18}F-FDG PET/CT scans from 25 patients with clinically active Crohn disease and correlated the findings to endoscopic procedures performed within 5 d before or after CT without any interfering treatment. The colon was divided into ileocecum, ascending colon, colon transversum, descending colon, and rectosigmoid segments, so that 125 colonic segments were analyzed. The extent of mucosal lesions was categorized into deep ulcerations, superficial ulcerations, erythema, or unaffected for each individual segment. PET/CT was considered positive if the SUV_{max} for the segment analyzed was higher than 4 (*22*). Interestingly, we assessed positive PET/CT findings in most extensive ulcerations (88%). In contrast, only about 50% of superficial epithelial lesions were found positive by PET/CT, not differing from the detection rate found for lesions without any epithelial damage but showing erythema (58%). Finally, 16% of the segments analyzed having endoscopic regularly appearing mucosa exhibited an enhanced ^{18}F-FDG uptake (Fig. 6).

DISCUSSION

In this study, we present ^{18}F-FDG PET/CT as a noninvasive approach to assess murine DSS colitis. Colonic ^{18}F-FDG uptake correlated strongly to established parameters such as histologic inflammation score and weight loss. In addition, we correlated endoscopic lesions in IBD patients to ^{18}F-FDG uptake assessed by PET/CT. We herein show the feasibility of ^{18}F-FDG PET/CT for the evaluation of murine colitis and propose that this method might extend the detection of ongoing inflammation in Crohn disease.

Because intestinal inflammatory pathways cannot readily be simulated, in vitro animal models are generally used to study the relevance of, for example, genetic knock-outs or new therapeutic agents. However, to avoid necropsy and histologic examinations, the quantification of the inflammatory process usually addresses surrogate markers such as diarrhea, hematochezia, and weight loss. Although they can repeatedly be measured, these parameters do not necessarily reflect the ongoing active immune response. In addition,

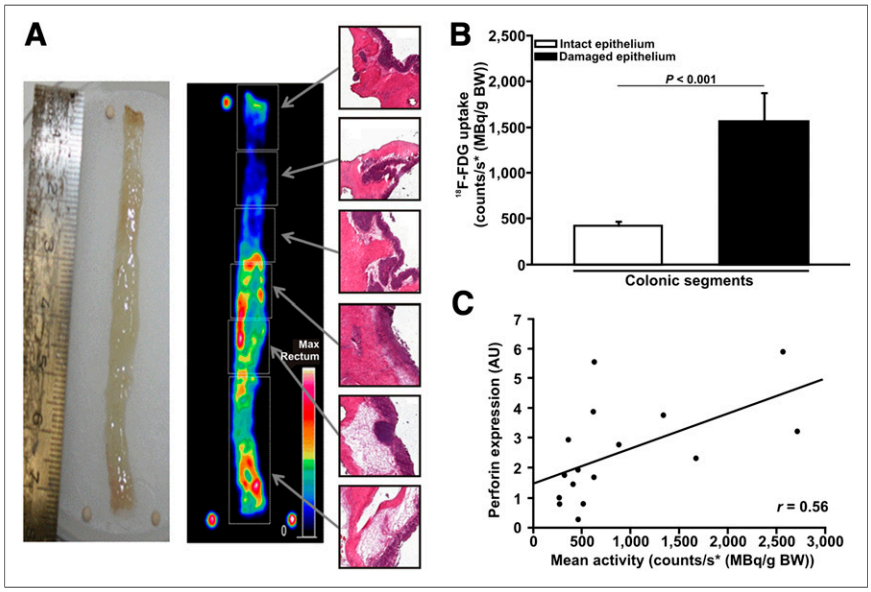

FIGURE 5. Correlation of ^{18}F-FDG uptake to histologic epithelial damage and mucosal cellular infiltrate. (A) ^{18}F-FDG uptake in vivo was assessed by PET of explanted colons and analyzed using standardized VOIs (white boxes). One-centimeter colon pieces were again divided and transferred to hematoxylin and eosin staining and PCR analysis. (B) Comparison of ^{18}F-FDG uptake in intact vs. damaged epithelium in WT mice 10 d after DSS application. (C) Correlation of segmental ^{18}F-FDG uptake in colon with corresponding mucosal relative expression of perforin measured by real-time PCR ($P = 0.02$). BW = body weight; max = maximum.

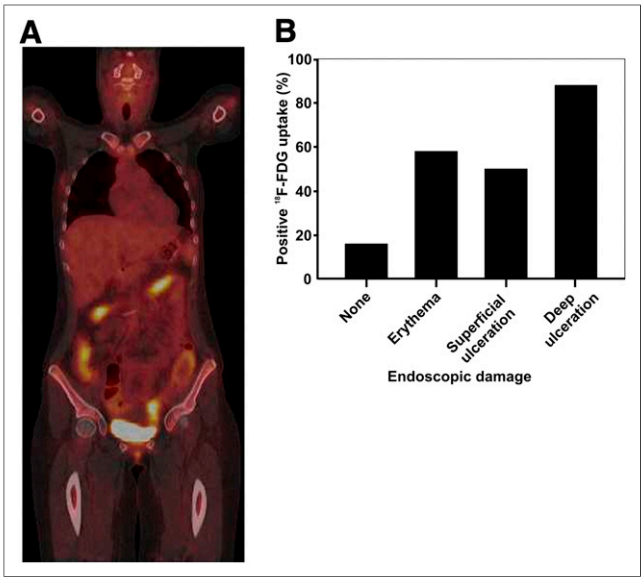

FIGURE 6. Correlation of ^{18}F-FDG uptake to endoscopic findings. Correlation of standardized uptake value–based positive ^{18}F-FDG uptake in colonic segments of 25 patients with Crohn disease to findings of subsequently performed colonoscopy.

the localization of active inflammation can generally not be determined because endoscopic examinations in mice are limited.

Molecular imaging has evolved in this field because a single animal can repeatedly be studied over time, thereby limiting the number of mice needed for performance of individual measurements during the follow-up. Recently, Hindryckx et al. demonstrated that ^{18}F-FDG PET/CT was able to detect DSS-induced intestinal inflammation and correlated strongly with histologic examinations (*9*). In accordance with these observations, we were able to detect a good correlation of ^{18}F-FDG PET/CT to histologic alterations at the maximum of inflammation and also in the phase of recovery. In addition, ^{18}F-FDG PET/CT enabled us to locally quantify the inflammatory process in distinct anatomic parts of the intestine.

Previously, Hindryckx et al. reported a 100% correlation of the PET signal to myeloperoxidase levels, suggesting that neutrophil infiltration might rather be the source of the signal detected in DSS colitis supported by several earlier observations (*9*). In addition, it has been shown that initiation of acute DSS colitis is predominantly mediated by neutrophils (*13*). In line with these findings, we detected a strong correlation between increased ^{18}F-FDG uptake and epithelial damage, which is histologically associated with neutrophil infiltration. Moreover, we found a significantly enhanced metabolic activation within multiple major joints induced by hyperplasia of immature neutrophils within the bone marrow of DSS-treated animals. The activation significantly correlated to the ongoing intestinal inflammation, which was also predominantly mediated by neutrophils and macrophages. It also can be speculated that arthralgia associated with active IBD might occasionally be induced by reactive bone marrow hyperplasia as observed, for example, after granulocyte colony-stimulating factor treatment (*24*). In contrast, data from Brewer et al. demonstrated that $CD4^+$ T cells might be the cellular source of the increased ^{18}F-FDG uptake in chronic intestinal inflammation (*25*). Confirmatively, we found a robust correlation between mucosal T cell infiltration and ^{18}F-FDG uptake. Taken together, these findings may reflect changes in cellular mucosal composition over the course of colitis. Whereas initiation of colonic inflammation is mainly mediated by neutrophils, the ongoing inflammation is additionally orchestrated by T cells. This evolving nature of the inflammatory mucosal infiltrate may explain why no singular correlation between one cell type and ^{18}F-FDG uptake was observed.

Recently, ^{18}F-FDG PET/CT has also been studied in human IBD, although some concerns have to be raised on the radiation exposure in rather young patients. It is also unclear in which clinical context PET/CT might be a reasonable tool to study human IBD. In ulcerative colitis, the correlation of disease activity and PET/CT has been shown to be as high as 95% (*26*). Because the activity of ulcerative colitis is limited to the colon, and the mucosal damage can be easily determined by partial colonoscopy, the benefit for the diagnosis of ulcerative colitis is currently rather limited. Previous data could also show that severe lesions in Crohn disease are readily detectable by this method (*27*). However, minor alterations such as superficial ulcerations and erythema have been detected only in about 72% and 50%, respectively (*27*). Indeed, it has been demonstrated that the quantification of the intestinal glucose uptake as measured by ^{18}F-FDG PET/CT is quite variable, and pathologic findings are sometimes not readily differentiable from regular intestinal segments. By using SUV_{max} as published previously by Toriihara et al. (*28*) as a cutoff value, we were also only able to detect 50% of superficial ulcerations and 58% of erythema, indicating that endoscopic evaluations are favorable to characterize mucosal disease activity. Corresponding with the clinical data, the increase of glucose metabolism observed within DSS-induced lesions without epithelial defects was as low as 20% from baseline. Given the quite significant differences in metabolic activity of the human colon, it seems to be unlikely that minor mucosal alterations can sufficiently be detected by PET/CT. However, a substantial amount of Crohn disease patients showed significantly enhanced glucose metabolism in the colon although no endoscopic lesions were visible, and a similar percentage has also been reported previously (*27*). The data suggest that in some patients the transmural inflammatory process might not be noticeable by endoscopy. It is therefore necessary to evaluate in future studies whether patients with ongoing ^{18}F-FDG PET/CT activity are at risk for an unfavorable disease outcome such as early relapse or stricture formation. Because evolving treatment strategies are focusing on changing the disease behavior by inducing a deep remission, it might therefore also be reasonable to include ^{18}F-FDG PET/CT in the diagnostic repertoire of Crohn disease.

CONCLUSION

^{18}F-FDG PET/CT is a noninvasive method for evaluation of both experimental colitis and Crohn disease patients and thereby offers promising translational potential.

DISCLOSURE

The costs of publication of this article were defrayed in part by the payment of page charges. Therefore, and solely to indicate this fact, this article is hereby marked "advertisement" in accordance with 18 USC section 1734. This work was supported by grants from the DFG (KO2155/2-2), the Sonderforschungsbereich 656 (SFB 656 C7) and the Interdisciplinary Center of Clinical Research (IZKF core unit PIX), Münster, Germany. No other potential conflict of interest relevant to this article was reported.

ACKNOWLEDGMENTS

We are grateful to Sonja Dufentester, Elke Weber, Ute Neugebauer, Richard Stadermann, and Dominik Kentrup for excellent technical assistance.

REFERENCES

1. Vucelic B. Inflammatory bowel diseases: controversies in the use of diagnostic procedures. *Dig Dis.* 2009;27:269–277.
2. Baumgart DC, Sandborn WJ. Inflammatory bowel disease: clinical aspects and established and evolving therapies. *Lancet.* 2007;369:1641–1657.
3. Rodríguez-Reyna TS, Martinez-Reyes C, Yamamoto-Furusho JK. Rheumatic manifestations of inflammatory bowel disease. *World J Gastroenterol.* 2009;15:5517–5524.
4. Henriksen M, Jahnsen J, Lygren I, et al. C-reactive protein: a predictive factor and marker of inflammation in inflammatory bowel disease: results from a prospective population-based study. *Gut.* 2008;57:1518–1523.
5. Bitton A, Peppercorn MA, Antonioli DA, et al. Clinical, biological, and histologic parameters as predictors of relapse in ulcerative colitis. *Gastroenterology.* 2001;120:13–20.
6. Baert F, Moortgat L, Van Assche G, et al. Mucosal healing predicts sustained clinical remission in patients with early-stage Crohn's disease. *Gastroenterology.* 138:463–468; quiz e410-461.
7. Byrne FR, Viney JL. Mouse models of inflammatory bowel disease. *Curr Opin Drug Discov Devel.* 2006;9:207–217.
8. Kaser A, Zeissig S, Blumberg RS. Inflammatory bowel disease. *Annu Rev Immunol.* 2010;28:573–621.
9. Hindryckx P, Staelens S, Devisscher L, et al. Longitudinal quantification of inflammation in the murine dextran sodium sulfate-induced colitis model using muPET/CT. *Inflamm Bowel Dis.* 2011;17:2058–2064.
10. Meller J, Sahlmann CO, Scheel AK. ^{18}F-FDG PET and PET/CT in fever of unknown origin. *J Nucl Med.* 2007;48:35–45.
11. Spier BJ, Perlman SB, Jaskowiak CJ, Reichelderfer M. PET/CT in the evaluation of inflammatory bowel disease: studies in patients before and after treatment. *Mol Imaging Biol.* 2010;12:85–88.
12. Spier BJ, Perlman SB, Reichelderfer M. FDG-PET in inflammatory bowel disease. *Q J Nucl Med Mol Imaging.* 2009;53:64–71.
13. Okayasu I, Hatakeyama S, Yamada M, Ohkusa T, Inagaki Y, Nakaya R. A novel method in the induction of reliable experimental acute and chronic ulcerative colitis in mice. *Gastroenterology.* 1990;98:694–702.
14. Dieleman LA, Palmen MJ, Akol H, et al. Chronic experimental colitis induced by dextran sulphate sodium (DSS) is characterized by Th1 and Th2 cytokines. *Clin Exp Immunol.* 1998;114:385–391.
15. Egger B, Bajaj-Elliott M, MacDonald TT, Inglin R, Eysselein VE, Buchler MW. Characterisation of acute murine dextran sodium sulphate colitis: cytokine profile and dose dependency. *Digestion.* 2000;62:240–248.
16. Pellegrino D, Bonab AA, Dragotakes SC, Pitman JT, Mariani G, Carter EA. Inflammation and infection: imaging properties of ^{18}F-FDG-labeled white blood cells versus ^{18}F-FDG. *J Nucl Med.* 2005;46:1522–1530.
17. Reuter S, Schnockel U, Schroter R, et al. Non-invasive imaging of acute renal allograft rejection in rats using small animal F-FDG-PET. *PLoS ONE.* 2009;4: e5296.
18. Bettenworth D, Buyse M, Bohm M, et al. The Tripeptide KdPT protects from intestinal inflammation and maintains intestinal barrier function. *Am J Pathol.* 2011;179:1230–1242.
19. Schäfers KP, Reader AJ, Kriens M, Knoess C, Schober O, Schafers M. Performance evaluation of the 32-module quadHIDAC small-animal PET scanner. *J Nucl Med.* 2005;46:996–1004.
20. Zwerina J, Redlich K, Polzer K, et al. TNF-induced structural joint damage is mediated by IL-1. *Proc Natl Acad Sci USA.* 2007;104:11742–11747.
21. Koschmieder S, Gottgens B, Zhang P, et al. Inducible chronic phase of myeloid leukemia with expansion of hematopoietic stem cells in a transgenic model of BCR-ABL leukemogenesis. *Blood.* 2005;105:324–334.
22. Toriihara A, Yoshida K, Umehara I, Shibuya H. Normal variants of bowel FDG uptake in dual-time-point PET/CT imaging. *Ann Nucl Med.* 2011;25:173–178.
23. Mary JY, Modigliani R. Development and validation of an endoscopic index of the severity for Crohn's disease: a prospective multicentre study. Groupe d'Etudes Therapeutiques des Affections Inflammatoires du Tube Digestif (GETAID). *Gut.* 1989;30:983–989.
24. Gonçalves A, Viret F, Ciccolini J, et al. Phase I and pharmacokinetic study of escalating dose of docetaxel administered with granulocyte colony-stimulating factor support in adult advanced solid tumors. *Clin Cancer Res.* 2003;9:102–108.
25. Brewer S, McPherson M, Fujiwara D, et al. Molecular imaging of murine intestinal inflammation with 2-deoxy-2-[^{18}F]fluoro-D-glucose and positron emission tomography. *Gastroenterology.* 2008;135:744–755.
26. Meisner RS, Spier BJ, Einarsson S, et al. Pilot study using PET/CT as a novel, noninvasive assessment of disease activity in inflammatory bowel disease. *Inflamm Bowel Dis.* 2007;13:993–1000.
27. Louis E, Ancion G, Colard A, Spote V, Belaiche J, Hustinx R. Noninvasive assessment of Crohn's disease intestinal lesions with ^{18}F-FDG PET/CT. *J Nucl Med.* 2007;48:1053–1059.
28. Chandler MB, Zeddun SM, Borum ML. The role of positron emission tomography in the evaluation of inflammatory bowel disease. *Ann N Y Acad Sci.* 2011;1228:59–63.